

# RSC Advances



This is an *Accepted Manuscript*, which has been through the Royal Society of Chemistry peer review process and has been accepted for publication.

*Accepted Manuscripts* are published online shortly after acceptance, before technical editing, formatting and proof reading. Using this free service, authors can make their results available to the community, in citable form, before we publish the edited article. This *Accepted Manuscript* will be replaced by the edited, formatted and paginated article as soon as this is available.

You can find more information about *Accepted Manuscripts* in the [Information for Authors](#).

Please note that technical editing may introduce minor changes to the text and/or graphics, which may alter content. The journal's standard [Terms & Conditions](#) and the [Ethical guidelines](#) still apply. In no event shall the Royal Society of Chemistry be held responsible for any errors or omissions in this *Accepted Manuscript* or any consequences arising from the use of any information it contains.

# Two Luminescent Metal-Organic Frameworks with Multifunctional Properties for Nitroaromatic Compounds Sensing and Photocatalysis

Fengqin Wang<sup>1\*</sup>, Chengmiao Wang<sup>1</sup>, Zongchao Yu<sup>1</sup>, Qingguo He<sup>2</sup>, Xiuyu Li<sup>1</sup>, Chonglong Shang<sup>1</sup>, Yongnan Zhao<sup>3</sup>

<sup>1</sup>College of Environment and Chemical Engineering & Key Lab of Hollow Fiber Membrane Materials & Membrane Process, Tianjin Polytechnic University, Tianjin 300387, China

<sup>2</sup>State Key Lab of Transducer Technology, Shanghai Institute of Microsystem and Information Technology, Chinese Academy of Sciences, Changning Road 865, Shanghai 200050, China.

<sup>3</sup>College of Materials and Engineering & Key Lab of Hollow Fiber Membrane Materials & Membrane Process, Tianjin Polytechnic University, Tianjin 300387, China

E-mail: wangfengqin@tjpu.edu.cn Tel: (+86)-22-83955457

**ABSTRACT:** Two new luminescent metal-organic frameworks (MOFs), [Zn(L)<sub>0.5</sub>(1,10-phen)(H<sub>2</sub>O)].2H<sub>2</sub>O (**1**) and [Cd(L)<sub>0.5</sub>(1,10-phen)(H<sub>2</sub>O)].2H<sub>2</sub>O (**2**), have been successfully synthesized using bis-(3,5-dicarboxyphenyl)terephthalamide (H<sub>4</sub>L) as organic linkers and 1,10-phen as auxiliary ligand under solvothermal conditions. The two complexes are isostructural and they both have 1D ladder chain structures. For the two complexes, the participation of the fluorescent ligand H<sub>4</sub>L not only gives rise to a strong photoluminescence emission as expected, but more interestingly, that ligand originated characteristic band could be quenched selectively by nitroaniline with a low detection limit. The results show that **1** and **2** can be promising fluorescence sensors for selective detecting and recognizing nitroaromatic compounds via fluorescence quenching mechanism. Meanwhile, the photocatalytic activities were also determined by UV lightinduced photodegradation of Rhodamine B (RhB) experiments. The obtained results indicate that **1** and **2** can be stable and good UV light driving heterogeneous photocatalyst, which can be used to treat effectively wastewater of organic dyes in the future.

**Keywords:** Metal-organic Framework, Fluorescence sensing, Nitroaromatic compound, Photocatalysis

## 1. Introduction

Metal-organic frameworks (MOFs) have been an active research field and receiving considerable attention not only for their aesthetically beautiful architectures but also for their potential applications in numerous areas. Up to now, a variety of MOFs have been successfully constructed for the applications in gas storage<sup>1</sup> and separation<sup>2</sup>, heterogeneous catalysis<sup>3</sup>, chemical sensing<sup>4</sup> and so on. Among these potential applications, fluorescence detection based on MOF chemical sensors has been proven to be an excellent candidate for rapid recognition and sensing of nitroaromatic compounds due to their advantages of high sensibility, simplicity and short response time. Moreover, nitroaromatic compounds are not only well-known explosives but also notorious environmental pollutants. Therefore, developing highly sensitive and selective fluorescence sensors for rapid and effective detection of nitroaromatic compounds is an extremely urgent issue concerning homeland security, environmental protection and humanitarian concerns. The first work for detecting of nitroaromatic compounds by MOF-based fluorescence sensor appeared only in 2009.<sup>5</sup> After that, fluorescence MOFs as explosive detectors represent a brand new sub-field of MOF research and some MOFs with fluorescence quenching ability have been designed and used for recognition and detection of electron-deficient nitroaromatic molecules.<sup>6,7</sup> However, it is still at the early stage comparing with the other applications.

In addition, MOFs have also received considerable attention for their applications as a new kind of promising photocatalyst in purifying water by thoroughly decomposing organic dyes because of their high surface areas and high light absorption abilities. Moreover, the photodegradation is an efficient and economical way to decompose organic dyes into less dangerous products comparing to the other methods.<sup>8</sup> In general, MOFs with absorption bands in the UV region exhibit photocatalytic performance for degrading organic dyes upon UV light excitation. Recently, some literatures have reported the applications of heterogeneous photodegradation of organic dyes.<sup>9</sup> However, the MOFs reported so far exhibit mainly mono-functionality except that only a few examples have reported the

applications of multifunctionality.<sup>10</sup> Therefore, it is still a challenge to construct multifunctional framework materials by selecting the proper organic ligands with aromatic moieties as linkers and transition metal centers as nodes.

As the continuous our work, two luminescent MOFs,  $[\text{Zn}(\text{L})_{0.5}(\text{1,10-phen})(\text{H}_2\text{O})] \cdot 2\text{H}_2\text{O}$  (**1**) and  $[\text{Cd}(\text{L})_{0.5}(\text{1,10-phen})(\text{H}_2\text{O})] \cdot 2\text{H}_2\text{O}$  (**2**) have been successfully synthesized using bis-(3,5-dicarboxyphenyl) terephthalamide ( $\text{H}_4\text{L}$ ) as the organic linker and 1,10-phen as auxiliary ligand. Herein, we reported the structures of them and studied the fluorescence sensing performance as well as the photocatalytic activity of the two MOFs. The X-ray diffraction analyses reveal that complexes **1** and **2** are isostructural and both exhibit 1D ladder chain metal-organic framework. The fluorescence sensing experiments demonstrate that the two MOFs display sensitive selectivity toward nitroaniline in solution phase via fluorescence quenching effect, which can be potentially used for pollutants detection or environmental monitoring. In addition, complexes **1** and **2** also exhibit good photocatalytic activity in the green degradation of organic dyes under UV light irradiation.

## 2. Experimental section

### 2.1 General procedures

All the reagents were obtained from commercial sources and used as received. *bis*-(3,5-dicarboxyphenyl)terephthalamide ( $\text{H}_4\text{L}$ ) was prepared according to the literature.<sup>11</sup> Infrared spectra were recorded on a FTIR-650 system using KBr pellets in the range 4000 – 400  $\text{cm}^{-1}$ . Elemental analyses (C, H and N) were measured on a Perkin-Elmer auto-analyzer. Thermogravimetric (TG) analysis was carried out on a Netzsch STA 409 PG/PC analyzer at a heating rate of 5  $^\circ\text{C min}^{-1}$  from ambient temperature to 800  $^\circ\text{C}$ . Powder X-ray diffraction (PXRD) data was recorded on a D/MAX-2500 automated diffractometer. The simulated PXRD pattern was derived from the single crystal data through the diffraction-crystal module of the Mercury program version 3.0. The photoluminescence spectra of the complexes studied in the solid state and their samples in DMA or isopropanol solution were measured on an

F-380 spectrophotometer. The solid-state diffuse-reflectance spectra for powdered samples were recorded on a U-4100 spectrophotometer spectrometer equipped with an integrating sphere using BaSO<sub>4</sub> as a white standard. The UV/Vis adsorption spectra were recorded using an Evolution 201 UV-vis spectrometer.

## 2.2 Synthesis of [Zn(L)<sub>0.5</sub>(1,10-phen)(H<sub>2</sub>O)]·2H<sub>2</sub>O (**1**)

A mixture of H<sub>4</sub>L (24.6 mg, 0.05 mmol), ZnSO<sub>4</sub>·7H<sub>2</sub>O (28.7 mg, 0.1 mmol), 1,10-phen (18.0 mg, 0.1 mmol), DMF (2 mL) and H<sub>2</sub>O (2 mL) and 0.1 mL concentrated HNO<sub>3</sub> were sealed in a 25mL stainless steel vessel and heated at 85 °C for 3 days under autogenous pressure, and then cooled to room temperature. Colorless block crystals of **1** were obtained by filtration. Yield: 86.7% based on Zn. Elemental analysis (%) calcd for C<sub>24</sub>H<sub>20</sub>N<sub>3</sub>O<sub>8</sub>Zn: C, 52.96; H, 3.68; N, 7.72. Found: C, 53.13; H, 3.34; N, 7.26. IR (KBr pellet cm<sup>-1</sup>): 3432 br, 1642 s, 1590 s, 1450 s, 1355 vs, 1103 m, 1024 m, 868 s, 781 s, 729 m, 615 w, 520 w.

## 2.3 Synthesis of [Cd(L)<sub>0.5</sub>(1,10-phen)(H<sub>2</sub>O)]·2H<sub>2</sub>O (**2**)

A mixture of H<sub>4</sub>L (24.6 mg, 0.05 mmol), CdCl<sub>2</sub>·5/2H<sub>2</sub>O (22.8 mg, 0.1 mmol), 1,10-phen (18.0 mg, 0.1 mmol), DMF (4 mL) and H<sub>2</sub>O (4 mL) and 0.1 mL concentrated HNO<sub>3</sub> were sealed in a 25 mL stainless steel vessel and heated at 85 °C for 3 days under autogenous pressure, and then cooled to room temperature. Colorless block crystals of **2** were obtained by filtration. Yield: 76.7% based on Cd. Elemental analysis (%) calcd for C<sub>24</sub>H<sub>20</sub>CdN<sub>3</sub>O<sub>8</sub>: C, 48.78; H, 3.39; N, 7.11. Found: C, 49.05; H, 3.16; N, 7.02. IR (KBr pellet cm<sup>-1</sup>): 3350 br, 1630 vs, 1554 s, 1493 m, 1433 s, 1358 s, 1102 m, 990 w, 855 m, 773 s, 720 s, 622 w, 501 w.

## 2.4 Fluorescence titrations in dispersed medium

To examine the potential of **1** and **2** for sensing nitroaromatic compounds, the MOFs (3 mg) were immersed in DMA (3 mL) for **1** and isopropanol (3 mL) for **2**, respectively, which were treated by ultrasonication for 1.5 h. All titrations were carried out by gradually adding analytes in an incremental fashion. The corresponding fluorescence emission spectra were recorded at 298 K. Each titration was repeated several times to get concordant values. For all measurements, the suspensions of **1** were excited at  $\lambda_{\text{ex}} = 330$  nm and the corresponding emission wavelengths were

monitored from 340 to 650 nm. The suspensions of **2** were excited at  $\lambda_{\text{ex}} = 318$  nm and the corresponding emission wavelengths were monitored from 330 to 600 nm. The fluorescence efficiency was calculated by using the formula  $[(F_0-F)/F_0] \times 100\%$  ( $F_0$  is the initial fluorescence intensity). Fluorescence quenching titration was further evaluated using the Stern–Volmer equation  $F_0/F = 1 + K_{\text{sv}}[M]$ , where the values  $F_0$  and  $F$  are the fluorescence intensity of the MOFs suspension without and with addition of analytes, respectively,  $K_{\text{sv}}$  is the quenching constant,  $[M]$  is the analytes concentration.

### 2.5 Photocatalytic experiments

Photocatalytic experiments in aqueous solutions were performed in a 150 mL quartz beaker. A 500 W high-pressure mercury lamp was used as the UV light source. An aqueous solution of RhB (80 mL) with a concentration of  $10^{-5}$  mol·L<sup>-1</sup> was mixed with the catalysts (20 mg) and illuminated. Before turning on the lamp, the suspension containing RhB and the photocatalyst was magnetically stirred in the dark for 40 min until an adsorption-desorption equilibrium was established. At given irradiation intervals, a series of aqueous solutions of a certain volume were collected and separated by centrifugation to remove suspended catalyst particles and then subjected to UV/Vis spectroscopic measurements.

### 2.6 X-ray crystallography

Single crystal X-ray diffraction measurements for **1** and **2** were carried out on computer-controlled Bruker SMART 1000 CCD diffractometer equipped with graphite-monochromatized Mo-K $\alpha$  with a radiation wavelength of 0.71073 Å using the  $\omega$ -scan technique. The structures were solved by direct methods and refined by full-matrix least squares on  $F^2$  using the SHELXS 97 and SHELXL 97 programs.<sup>12</sup> Semiempirical absorption corrections were applied using the SADABS program.<sup>13</sup> All non-hydrogen atoms were refined anisotropically. The hydrogen atoms were generated geometrically and treated by a mixture of independent or constrained refinement. The crystallographic data for **1** and **2** are listed in Table S1, and selected bond lengths (Å) and angles (°) are listed in Table S2.

### 3. Results and discussion

#### 3.1 Structural characterization

Single crystal X-ray diffraction determinations show that complexes **1** and **2** are isostructural. So, only the structure of **1** will be discussed in detail. The asymmetric unit of **1** consists of one independent zinc ion, two L ligands, one 1,10-phen molecule, one coordinated water molecules and two guest water molecules. The coordination environment of Zn (II) ion is shown in Fig. 1. The Zn ion is six-coordinated with a  $\text{N}_2\text{O}_4$  donor set, three oxygen atoms coming from the carboxylate groups of two different L ligands, the remaining one oxygen atom from one coordinated water molecule, and two nitrogen atoms from one 1,10-phen molecule. The coordination environment of Zn (II) ion can be described as a distorted octahedron geometry. The Zn–O distances are in the range of 2.0408 – 2.3191 Å. The Zn–N distances are 2.1097(17) and 2.1597(17) Å, respectively.

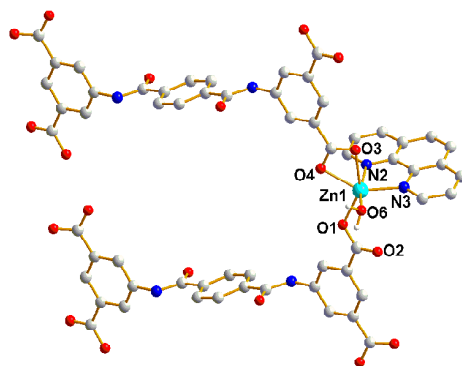


**Fig. 1** The coordination environment of Zn (II) ion in **1** with 30% probability thermal ellipsoids.

In complex **1**, all the four carboxylate groups of L ligand are deprotonated. The two terminal isophthalic moieties are coplanar, which are nearly perpendicular to the central terephthalic. The dihedral angle is 89.11 and 89.17°, respectively. And also, each L ligand adopts bidentate chelating and monodentate mode to link four Zn (II) ions into 1D ladder chain along a-axis, which contains a 38-membered ring with two Zn atoms, as shown in Fig. 2a. In these 1D chains, the phen molecules lie in the two sides, and nearly perpendicular to the isophthalic moieties. Furthermore, these 1D chains are assembled into 3D supramolecular network (Fig. 2b) via hydrogen bonds and  $\pi$ - $\pi$  stacking interactions.

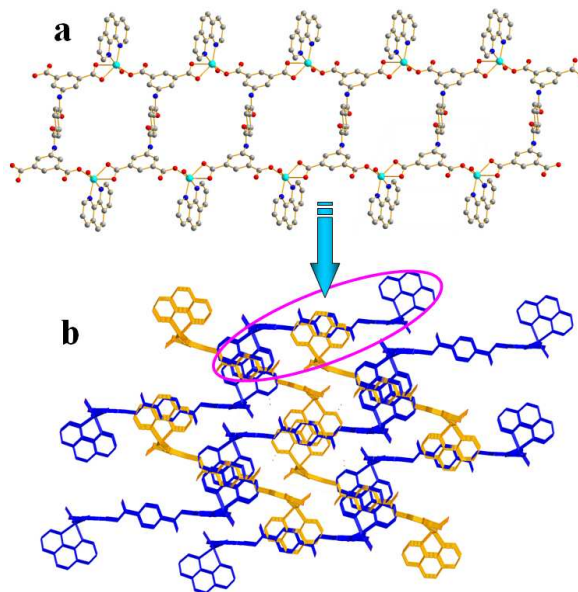


**Fig. 2** (a) The 1D ladder chain of **1** viewed along the a-axis. (b) The 3D supramolecular network of **1** containing the  $\pi$ - $\pi$  stacking interactions (the hydrogen bonds were excluded for clarity).

### 3.2 Thermal properties

The thermal stabilities of **1** and **2** were studied by thermogravimetric analysis (TGA). The thermal decomposition processes of them are similar. Taking **1** as an example, as observed from the TG curves, the thermal decomposition process occurred in three steps (Fig. S1 and S2). The first weight loss of 12.83% occurred between 100 and 200 °C, corresponding to the release of two coordinated water molecule and two free water molecules (calcd: 13.24%). With the temperature increasing, the framework started to collapse above 362 °C. The residue ZnO was obtained in 14.66% (calcd: 14.92%). In addition, the powder X-ray diffraction analyses of the two complexes were further conducted to confirm the phase purity of them (Fig. S3 and S4). The PXRD patterns of the as-synthesized sample of **1** and **2** are in good agreement with their corresponding simulated patterns, which indicate the phase purity of the synthesized samples.

### 3.3 The Photophysical Properties

The luminescent MOFs with different  $d^{10}$  metal ions have been the potential candidates for their excellent photoactive materials. Thereby, the solid-state

fluorescence spectra of **1** and **2** were recorded at room temperature. The maximum emission peaks of **1** and **2** are observed at 456 nm ( $\lambda_{\text{ex}} = 330$  nm) for **1** (Fig. S5) and 396 nm ( $\lambda_{\text{ex}} = 318$  nm) for **2** (Fig. S6), respectively. The emission spectra of **2** displays the obvious blue shift compared to that of L ligand ( $\lambda_{\text{em}} = 452$  nm and  $\lambda_{\text{ex}} = 357$  nm) (Fig. S7). This may be owed to substantial electronic coupling between the neighbor ligands through the  $d^{10}$  ( $\text{Zn}^{2+}$  or  $\text{Cd}^{2+}$ ) metal ions.<sup>14</sup> We also examined the fluorescence properties of **1** and **2** in common organic solvents. The emission wavelengths of **1** in DMA and **2** in isopropanol are similar to those of solid state samples (Fig. S8 and S9). The strong emissions of **1** and **2** in the solid state or in organic suspensions indicate their potential applications in liquid phase fluorescence detection.

### 3.4 Detection of nitroaromatic compounds

Based on the fluorescence properties of **1** and **2**, fluorescence detection experiments were carried out with DMA suspensions of **1** and isopropanol for **2** by gradually adding the small amounts of nitroaromatic compounds. The addition of nitroaromatic compounds, such as nitrobenzene, *p*-nitrotoluene, *m*-nitrotoluene and *p*-nitroaniline, lead to a distinct fluorescence quenching effect on the fluorescence intensity of the two MOFs. For the selected analytes, **1** and **2** show similar sensing behaviors. Among the given analytes, the quenching efficiency of *p*-nitroaniline is apparently larger than those of the others with the same concentration. When the added amount of *p*-nitroaniline was only 0.2  $\mu\text{mol}$ , the fluorescence intensity of **1** at 456 nm declined by 56.21% (Fig. 3a) and the fluorescence intensity of **2** at 396 nm declined by 59.63%, accompanied by a small red-shift to 456 nm (Fig. 3b). As shown in Fig. 3c and 3d, the linear correlation coefficient (*R*) in the  $K_{\text{sv}}$  curve suggest that the quenching effect of *p*-nitroaniline on the fluorescence of **1** and **2** fit the Stern–Volmer mode well. For the others, the quenching efficiencies for **1** and **2** are both obviously decreased (see Fig. S10-S15). The percentages of fluorescence quenching for the different analytes are given in Fig. 4a and 4b. Meanwhile, we took **1** as an example and study the effect of *p*-nitroaniline concentrations on the fluorescence intensity of **1**. As shown in Fig. 5, the concentration of *p*-nitroaniline has a remarkable influence on the fluorescence

intensity of **1**. When the concentration of *p*-nitroaniline was  $10^{-1} \text{ mol}\cdot\text{L}^{-1}$ , the quenched efficiency of **1** is about 85.36% with the addition amount of *p*-nitroaniline of only 5  $\mu\text{L}$ . However, with the concentration of *p*-nitroaniline decreasing from  $10^{-2}$  to  $10^{-4} \text{ mol}\cdot\text{L}^{-1}$ , the fluorescence quenching efficiency of **1** was decreased. The relationship between the fluorescence intensity of **1** and the concentrations of *p*-nitroaniline is in good agreement with the first-order exponential equation (insert of Fig. 5). These results indicate that **1** and **2** may be potential sensory materials for selective sensing of nitroaromatic compounds. And also, they are more sensitive to *p*-nitroaniline than other nitroaromatic compounds.

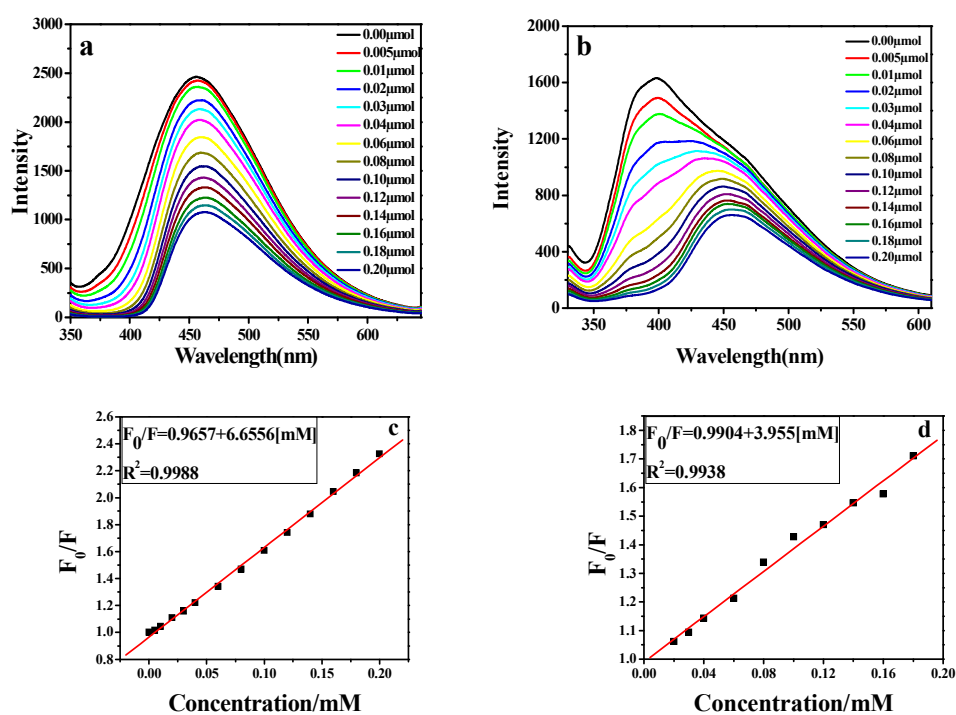


**Fig. 3** (a) Fluorescence titration of **1** dispersed in DMA with the addition of different volume of  $10^{-3} \text{ M}$  DMA solution of *p*-nitroaniline. The excitation wavelength was 330 nm and fluorescence emission was monitored from 340 to 650 nm. The slit width for both excitation and emission were 5 nm. (b) Fluorescence titration of **2** dispersed in isopropanol with the addition of different volume of  $10^{-3} \text{ M}$  isopropanol solution of *p*-nitroaniline. The excitation wavelength was 318 nm and fluorescence emission was monitored from 330 to 600 nm. The slit width for both excitation and emission were 5 nm. (c) The Stern-Volmer plot of **1** quenched by *p*-nitroaniline in DMA solution. (d) The Stern-Volmer plot of **2** quenched by *p*-nitroaniline in isopropanol solution.

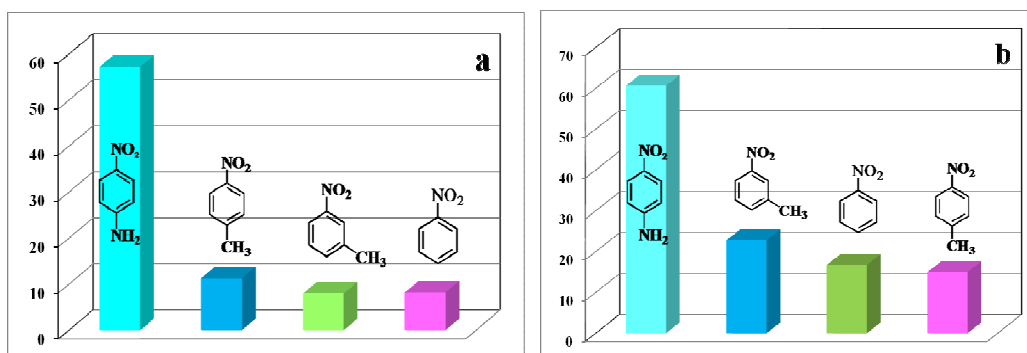


**Fig. 4** (a) Percentage of fluorescence quenching of **1** obtained for different analytes in DMA solution at room temperature; (b) Percentage of fluorescence quenching of **2** obtained for different analytes in isopropanol solution at room temperature.

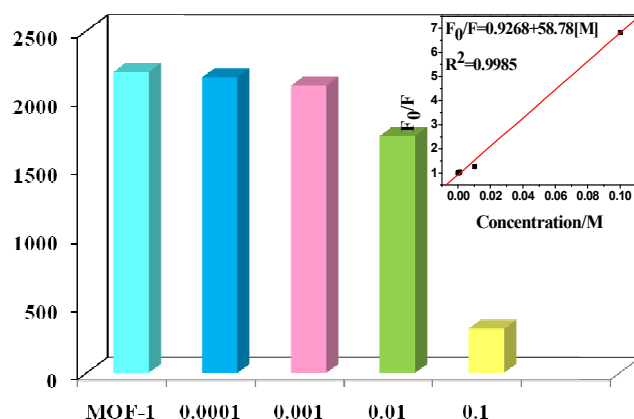


**Fig. 5** Fluorescence intensity of **1** obtained in DMA solution containing *p*-nitroaniline of different concentrations (excited at 330 nm and monitored from 340 to 650 nm.) The insert is Stern – Volmer plot of **1** quenched by *p*-nitroaniline in DMA solution.

From the crystal structures of **1** and **2**, we can find that the small pore size of these complexes might exclude their encapsulation of the targeted analytes, which indicates the sensing mechanism of our experiments might be different from most cases of guest-induced fluorescence response reported before.<sup>15</sup> Therefore, this fluorescence quenching might be attributed to the photoinduced electron transfer from electron-donating frameworks to electron-withdrawing analytes adsorbed on the surface of the MOFs. The selectivity of the two MOFs for different analytes could be caused by the electron-withdrawing effect of different substituent groups on the analytes and the effective interactions (such as hydrogen bonds and  $\pi$ - $\pi$  stacking)

between the MOFs and analytes. For *p*-nitroaniline, the -NH<sub>2</sub> groups as hydrogen bonds acceptor and donor, can take part in forming hydrogen bonds with MOFs and reinforce the  $\pi$ - $\pi$  stacking interactions between the framework of MOFs and benzene ring of *p*-nitroaniline. The cooperation of the two interactions induces facile intermolecular electron transfer and consequently leads to significant fluorescence quenching for the two MOFs in the presence of *p*-nitroaniline.<sup>16</sup> All the experimental results imply that the selectivity of the MOFs is related to the structures and electronic properties of both the MOFs and the analytes as well as the nature of their interactions. More indepth studies are required in order to fully understand the origin of the quenching effect.

### 3.5 Photocatalytic property study

The UV/Vis diffuse reflectance spectra measurements show that **1** and **2** both exhibit photoresponses in the UV light region. Calculations based on the Tauc equation give the band gaps ( $E_g$ ) of 3.40 eV for **1** and 3.31 eV for **2**, respectively (Fig. 6a and 6b). The absorption bands in UV light region make them potential materials to decomposition of organic dyes in UV light irradiation. Hence, the photocatalytic activities of the two MOFs were investigated by degradation of RhB in aqueous solution under UV light irradiation. In addition, controlled experiments on the photodegradation of RhB have also been carried out. Fig. 7 presents the comparisons of photocatalytic profiles of the samples under different conditions. Obviously, under dark condition or natural illumination (Fig. S16 and S17), the concentration of RhB almost does not change for every measurement in the presence of **1** and **2**. Illumination in the absence of **1** and **2** also does not result in the obvious photocatalytic decomposition of RhB. With the presence of photocatalysis and illumination, the absorption peaks of RhB have obviously decreased along with the prolonging of reaction time. The photocatalytic activities increase from 9.30% (without any catalyst) to 78.92% for **1**, 89.61% for **2** within 8 h, respectively (Fig. S18 and S19). These demonstrate that the presence of both illumination and MOFs is necessary for the degradation of RhB. And also, **2** exhibit higher photocatalytic activity than **1** under the same conditions. Although catalysts **1** and **2** possess the

same structures, different central metal ions between them may lead distinct bandgap sizes, which give rise to the discrepancy in their photocatalytic activities.<sup>17</sup> The kinetic data for degradation of RhB can be well fitted by the apparent first-order rate equation (Fig. 8). In addition, complex **1** was selected as an example to investigate the photostability under the irradiation of UV light. As shown in Fig. 9, the recycled **1** exhibit similar photodegradation performance with the parent compound **1**. The PXRD patterns and IR spectra of **1** were also monitored during the course of photocatalytic reactions. The PXRD patterns (Fig. 10) and IR (Fig. S20) spectra are nearly identical to those of the original compound **1**. These indicate that compound **1** is stable during photocatalysis and it can be used as stable photocatalyst for photodegradation of organic dyes. In addition, we also determined the IR spectra of **2** before and after photocatalysis (Fig. S21), the result demonstrates that compound **2** is also stable during photocatalysis.

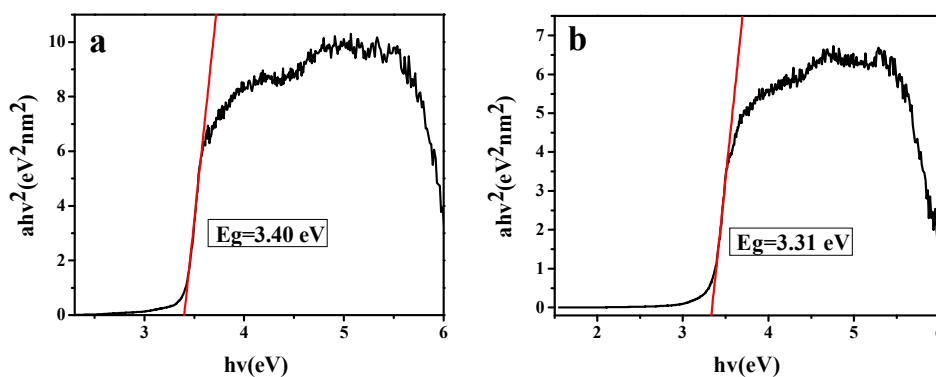


Fig. 6 Kubelka–Munk-transformed diffuse reflectance spectra of **1** (a) and **2** (b).

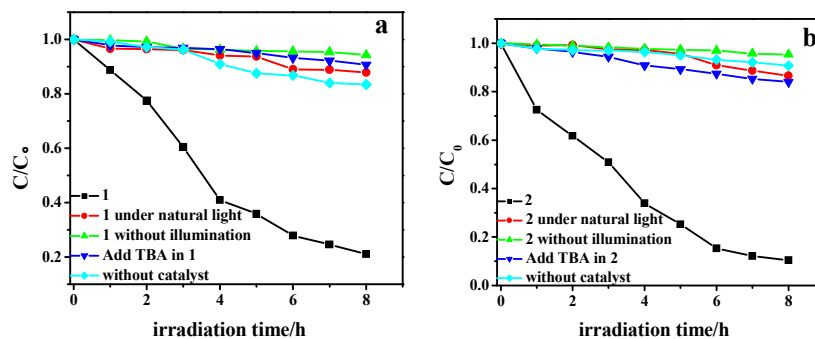


Fig. 7 The curves of degradation rate for RhB under different conditions of **1** (a) and **2** (b).

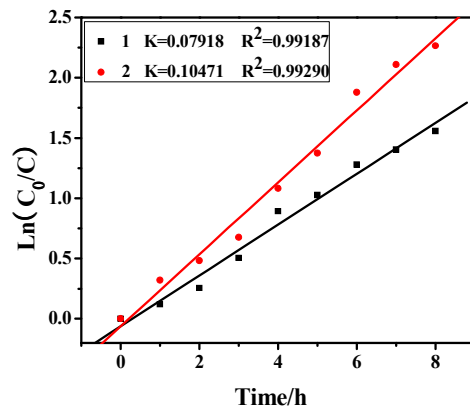


Fig. 8 The first-order plots for photodegradation RhB of 1 and 2.

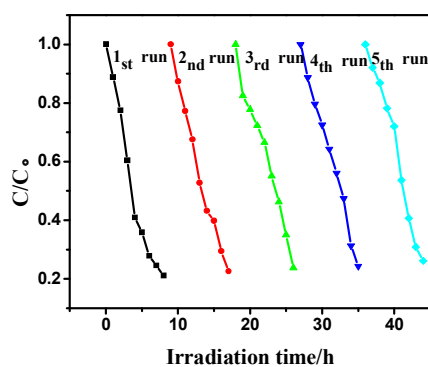


Fig. 9 Cycling runs of the photocatalytic degradation of RhB by 1 under UV light irradiation.

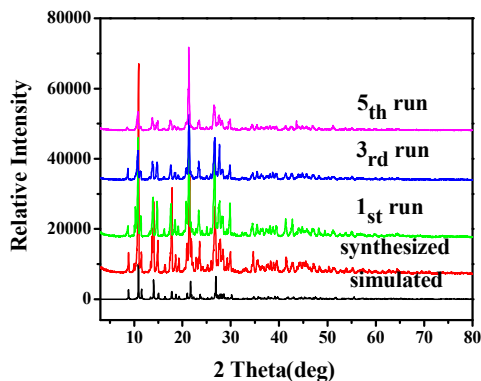
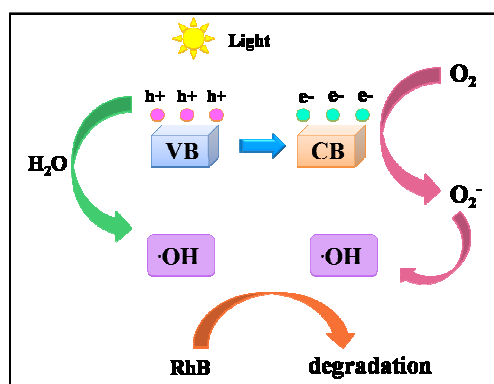


Fig. 10 PXRD patterns of 1 and recycled 1.

In our earlier work, the MOFs with photocatalytic activity are constructed from L ligand with Zn and Cd metal ions.<sup>9c,10b</sup> The degradation efficiencies were 47.9% and 17.1% under UV light irradiation for  $[\text{Zn}\cdot\text{L}]\cdot[\text{H}_2\text{N}(\text{CH}_3)_2]_2(\text{DMF})_{0.5}(\text{H}_2\text{O})_3$  and  $[\text{CdL}]\cdot[\text{H}_2\text{N}(\text{CH}_3)_2](\text{DMF})(\text{H}_2\text{O})_3$ , respectively, which are obviously lower than

those of complexes **1** and **2**. These results indicate that 1,10-phen ligand may decrease electronic band gap of the MOFs, which contribute greatly to the enhanced photocatalytic efficiencies.

In order to study the photocatalytic reaction mechanism, the photodegradation of RhB was carried out in the presence of 0.1 mmol tert-butyl alcohol (TBA), a widely used  $\cdot\text{OH}$  scavenger.<sup>19</sup> The presence of TBA greatly depressed the photodegradation rate of RhB on catalyst **1** and **2** (Fig. 7). For the two MOFs, the photocatalytic mechanism may be speculated as follows: under the irradiation of UV light, electrons can be excited from the valence band (VB) and transferred to the conduction band (CB) and simultaneously, positively charged holes are formed in the valence band. After migrating to the surface of MOFs, the electrons reduce the oxygen ( $\text{O}_2$ ) to the superoxide radical ( $\text{O}_2^-$ ) and the holes oxidize the hydroxyl ( $\text{H}_2\text{O}$ ) to hydroxyl radicals ( $\cdot\text{OH}$ ).<sup>18</sup> Therefore, one electron was captured from water molecules, which was oxygenated into the  $\cdot\text{OH}$  active species. Then the  $\cdot\text{OH}$  radicals could cleave RhB effectively to complete the photocatalytic process (Scheme 1).



**Scheme 1.** Schematic diagram of photocatalytic mechanism of complexes **1** and **2** under UV irradiation.

#### 4. Conclusions

In summary, two luminescent metal-organic frameworks (MOFs) have been successfully constructed from a tetradentate carboxylate ligand and 1,10-phen auxiliary ligand under solvothermal conditions. Encouraging by the good fluorescence emission and absorption band in UV light region of the two MOFs, we studied the

applications of the two MOFs in detection of nitroaromatic compounds and heterogeneous photocatalysis in detail. The sensing experiments indicate that the fluorescence emissions of the two MOFs are quenched by the selected nitroaromatic compounds to some extent. Among them, the *p*-nitroaniline exhibits the most significant fluorescence quenching performance to the MOFs. Besides, the two MOFs also exhibit effective UV-light driving photodegradation of RhB. The easily recoverable and reusable abilities make them good candidates for photodegradation of organic dyes. All the results suggest that **1** and **2** can serve as dual functional materials with chemical and photo stabilities for environment pollutant detection and heterogeneous photocatalyst.

### Acknowledgements

This project is supported by NSFC (Grant no. 21271138) and the NSF of Tianjin (No.14JCYBJC17500)

### Appendix A. Supplementary data

Crystallographic data in CIF (CCDC 1041268 and 1063105) or electronic supplementary information (ESI) available: TG of **1** and **2** (Fig. S1-2); PXRD of **1** and **2** (Fig. S3-4); Fluorescence spectra of **1**, **2** and ligand (Fig. S5-7); Emission spectra of **1** and **2** in different organic solvent (Fig. S8-9); Fluorescence titration spectra of **1** and **2** (Fig. S10-15); Absorption spectra of **1** and **2** under dark conditions, natural illumination, UV light and without any catalyst under UV light (Fig. S16-19); IR spectra of **1** and **2** before and after photocatalysis (Fig. S20-21).

### Notes and references

- (a) H. H. Wu, Q. H. Gong, D. H. Olson and J. Li, *Chem. Rev.*, 2012, **112**, 836-868; (b) M. Dincă and J. R. Long, *Angew. Chem. Int. Ed.*, 2008, **47**, 6766-6779; (c) L. J. Murray, M. Dincă and J. R. Long, *Chem. Soc. Rev.*, 2009, **38**, 1294-1314.
- (a) J. R. Li, J. Sculley and H. C. Zhou, *Chem. Rev.*, 2012, **112**, 869-932; (b) J. R. Li, R. J. Kuppler and H. C. Zhou, *Chem. Soc. Rev.*, 2009, **38**, 1477-1504; (c) P. S. Crespo, E. Stavitski, F. Kapteijna and J. Gascon, *RSC Adv.*, 2012, **2**, 5051-5053.
- (a) M. Yoon, R. Srirambalaji and K. Kim, *Chem. Rev.*, 2012, **112**, 1196-1231; (b) L.

- Q. Ma, C. Abney and W. B. Lin, *Chem. Soc. Rev.*, 2009, **38**, 1248-1256; (c) B. L. Chen, S. C. Xiang and G. D. Qian, *Acc. Chem. Res.*, 2010, **43**, 1115-1124; (d) Y. Liu, W. M. Xuan and Y. Cui, *Adv. Mater.*, 2010, **22**, 4112-4135.
- 4 (a) L. E. Kreno, K. Leong, O. K. Farha, M. Allendorf, R. P. Van Duyne and J. T. Hupp, *Chem. Rev.*, 2012, **112**, 1105-1125; (b) Y. J. Cui, Y. F. Yue, G. D. Qian and B. L. Chen, *Chem. Rev.*, 2012, **112**, 1126-1162; (c) M. D. Allendorf, C. A. Bauer, R. K. Bhakta and R. J. T. Houk, *Chem. Soc. Rev.*, 2009, **38**, 1330-1352; (d) J. Lee, O. K. Farha, J. Roberts, K. A. Scheidt, S. T. Nguyen and J. T. Hupp, *Chem. Soc. Rev.*, 2009, **38**, 1450-1459; (e) Q. B. Bo, H. Y. Wang, J. L. Miao and D. Q. Wang, *RSC Adv.*, 2012, **2**, 11650-11652.
- 5 A. J. Lan, K. H. Li, H. H. Wu, D. H. Olson, T. J. Emge, W. Ki, M. C. Hong and J. Li, *Angew. Chem. Int. Ed.*, 2009, **48**, 2334-2338.
- 6 (a) I. H. Park, R. Medishetty, J. Y. Kim, S. S. Lee and J. J. Vittal, *Angew. Chem. Int. Ed.*, 2014, **53**, 5591-5595; (b) D. Banerjee, Z. C. Hu, S. Pramanik, X. Zhang, H. Wang and J. Li, *CrystEngComm.*, 2013, **15**, 9745-9750; (c) Z. Hu, S. Pramanik, K. Tan, C. Zheng, W. Liu, X. Zhang, Y. J. Chabal and J. Li, *Cryst. Growth Des.*, 2013, **13**, 4204-4207; (d) A. J. Lan, K. H. Li, H. H. Wu, D. H. Olson, T. J. Emge, W. Ki, M. C. Hong and J. Li, *Angew. Chem. Int. Ed.*, 2009, **48**, 2334-2338; (e) S. Pramanik, C. Zheng, X. Zhang, T. J. Emge and J. Li, *J. Am. Chem. Soc.*, 2011, **133**, 4153-4155; (f) B. Gole, A. K. Bar and P. S. Mukherjee, *Chem. Eur. J.*, 2014, **20**, 2276-2291; (g) B. Gole, A. K. Bar and P. S. Mukherjee, *Chem. Eur. J.*, 2014, **20**, 13321-13336.
- 7 (a) Y. Zhao, J. M. Wang, H. Y. Liu and S. T. Gao, *J Inorg Organomet P.*, 2014, **24**, 1027-1031; (b) Z. H. Xiang, C. Q. Fang, S. H. Leng and D. P. Cao, *J. Mater. Chem. A.*, 2014, **2**, 7662-7665; (c) S. R. Zhang, D. Y. Du, J. S. Qin, S. L. Li, W. W. He, Y. Q. Lan and Z. M. Su, *Inorg. Chem.* 2014, **53**, 8105-8113; (d) X. Z. Song, S. Y. Song, S. N. Zhao, Z. M. Hao, M. Zhu, X. Meng, L. L. Wu and H. J. Zhang, *Adv. Funct. Mater.*, 2014, **24**, 4034-4041; (e) H. Wang, W. T. Yang and Z. M. Sun, *Chem. Asian J.*, 2013, **8**, 982-989; (f) S. N. Zhao, X. Z. Song, M. Zhu, X. Meng, L. L. Wu, S. Y. Song, C. Wang and H. J. Zhang, *RSC Adv.*, 2015, **5**,

- 93-98.
- 8 (a) D. Ravelli, D. Dondi, M. Fagnoni and A. Albini, *Chem. Soc. Rev.*, 2009, **38**, 1999-2011; (b) J. L. Wang, C. Wang and W. B. Lin, *ACS Catal.*, 2012, **2**, 2630-2640; (c) P. Mahata, G. Madras and S. Natarajan, *J. Phys. Chem. B.*, 2006, **110**, 13759-13768; (d) C. Wang, Z. G. Xie, K. E. deKrafft and W. B. Lin, *J. Am. Chem. Soc.*, 2011, **133**, 13445-13454; (e) L. H. Ai, C. H. Zhang, L. L. Li and J. Jiang, *Appl. Catal. B: Environ.*, 2014, **148-149**, 191-200.
- 9 (a) W. Q. Kan, B. Liu, J. Yang, Y. Y. Liu and J. F. Ma, *Cryst. Growth Des.* 2012, **12**, 2288-2298; (b) X. X. Xu, Z. P. Cui, J. Qi and X. X. Liu, *Dalton Trans.*, 2013, **42**, 4031-4039; (c) C. M. Wang, F. Q. Wang, C. F. Dong, Z. C. Yu, Z. C. Wang, Y. N. Zhao and G. D. Li, *Z. Anorg. Allg. Chem.*, 2015, **641**, 1125-1129; (d) D. Marcinkowski, M. Wałęsa-Chorab, M. Kubicki, M. Hoffmann, G. Kądziołka, B. Michalkiewicz and V. Patroniak, *Polyhedron.*, 2015, **90**, 91-98.
- 10 (a) X. L. Wang, J. Luan, H. Y. Lin, Q. L. Lu, M. Le, G. C. Liu and J. Y. Shao, *ChemPlusChem.*, 2014, **79**, 1691-1702; (b) F. Q. Wang, C. F. Dong, Z. C. Wang, Y. R. Cui, C. M. Wang, Y. N. Zhao and G. D. Li, *Eur. J. Inorg. Chem.*, 2014, **36**, 6239-6245; (c) Y. L. Wu, G. P. Yang, Y. Q. Zhao, W. P. Wu, B. Liu and Y. Y. Wang, *Dalton Trans.*, 2015, **44**, 3271-3277. (c) Z. J. Zhang, Y. G. Zhao, Q. H. Gong, Z. Li and J. Li, *Chem. Commun.*, 2013, **49**, 653-661; (d) S. L. Qiu and G. S. Zhu, *Coord. Chem. Rev.*, 2009, **253**, 2891-2911; (e) Q. R. Fang, G. S. Zhu, M. Xue, J. Y. Sun, F. X. Sun and S. L. Qiu, *Inorg. Chem.*, 2006, **45**, 3582-3587.
- 11 D. X. Hu and R. Kluger, *J. Biochem.*, 2008, **47**, 12551-12561.
- 12 (a) G. M. Sheldrick, SHELXS-97, Program for Crystal Structure Solution, University of Göttingen, Germany, 1997; (b) G. M. Sheldrick, SHELXL-97, Program for Crystal Structure Refinement, University of Göttingen, Germany, 1997.
- 13 G. M. Sheldrick, SADABS, Program for Empirical Absorption Correction of the Area detector Data, University of Göttingen, Germany, 1997.
- 14 (a) B. Gole, A. K. Bar and P. S. Mukherjee, *Chem. Eur. J.* 2014, **20**, 2276-2291; (b) W. H. Zhang, Z. Dong, Y. Y. Wang, L. Hou, J. C. Jin, W. H. Huang and Q. Z.

- Shi, *Dalton Trans.*, 2011, 40, 2509-2521; (c) Q. G. Wu, M. Esteghamatian, N. X. Hu, Z. Popovic, G. Enright, Y. Tao, M. D'Iorio and S. N. Wang, *Chem. Mater.*, 2000, **12**, 79-83; (d) J. E. McGarrah, Y. J. Kim, M. Hissler and R. Eisenberg, *Inorg. Chem.*, 2001, **40**, 4510-4511; (e) X. J. Zheng, L. P. Jin and S. Gao, *Inorg. Chem.*, 2004, **43**, 1600-1602; (f) H. Y. Bai, J. F. Ma, J. Yang, Y. Y. Liu, H. Wu and J. C. Ma, *Cryst. Growth Des.*, 2010, **10**, 995-1016; (g) H. Wu, H. Y. Liu, J. Yang, B. Liu, J. F. Ma, Y. Y. Liu and Y. Y. Liu, *Cryst. Growth Des.*, 2011, **11**, 2317-2324.
- 15 (a) L. Y. Zhang, L. Y. Sun, X. Y. Li, Y. L. Tian and G. Z. Yuan, *Dalton Trans.*, 2015, **44**, 401-410; (b) D. Banerjee, Z. C. Hu and J. Li, *Dalton Trans.*, 2014, **43**, 10668-10685; (c) M. Zhang, G. X. Feng, Z. G. Song, Y. P. Zhou, H. Y. Chao, D. Q. Yuan, T. T. Y. Tan, Z. G. Guo, Z. G. Hu, B. Z. Tang, B. Liu and D. Zhao, *J. Am. Chem. Soc.*, 2014, **136**, 7241-7244; (d) N. B. Shustova, T. C. Ong, A. F. Cozzolino, V. K. Michaelis, R. G. Griffin and M. Dincă, *J. Am. Chem. Soc.*, 2012, **134**, 15061-15070; (e) B. X. Zhang, J. L. Zhang, C. C. Liu, X. X. Sang, L. Peng, X. Ma, T. B. Wu, B. X. Han and G. Y. Yang, *RSC Adv.*, 2015, **5**, 37691-37696.
- 16 (a) L. Liu, J. Y. Hao, Y. T. Shi, J. S. Qiu and C. Hao, *RSC Adv.*, 2015, **5**, 3045-3053; (b) L. Liu, X. F. Chen, J. S. Qiu and C. Hao, *Dalton Trans.*, 2015, **44**, 2897-2906; (c) G. P. Yong, Y. Z. Li, Y. M. Zhang and W. L. She, *CrystEngComm.*, 2012, **14**, 1439-1448.; (d) G. Huang, C. Yang, Z. T. Xu, H. H. Wu, J. Li, M. Zeller, A. D. Hunter, S. S. Y. Chui and C. M. Che, *Chem. Mater.*, 2009, **21**, 541-546.
- 17 (a) L. L. Wen, F. Wang, J. Feng, K. L. Lv, C. G. Wang and D. F. Li, *Cryst. Growth Des.*, 2009, **9**, 3581-3589; (b) P. Du, Y. Yang, J. Yang, B. K. Liu and J. F. Ma, *Dalton Trans.*, 2013, **42**, 1567-1580; (c) J. Guo, J. Yang, Y. Y. Liu and J. F. Ma, *CrystEngComm.*, 2012, **14**, 6609.
- 18 (a) L. L. Wen, J. B. Zhao, K. L. Lv, Y. H. Wu, K. J. Deng, X. K. Leng and D. F. Li, *Cryst. Growth Des.*, 2012, **12**, 1603-1612; (b) S. Q. Zhang, L. Han, L. N. Li, J. Cheng, D. Q. Yuan and J. H. Luo, *Cryst. Growth Des.*, 2013, **13**, 5466-5472.

- 19 (a) Y. M. Xu and C. H. Langford, *Langmuir.*, 2001, **17**, 897-902; (b) Z. Xiong, Y. Xu, L. Zhu, J. Zhao, *Environ. Sci. Technol.*, 2005, **39**, 651-657; (c) M. Hu, Y. Xu,; J. Zhao, *Langmuir.*, 2004, **20**, 6302-6307.

## Two Luminescent Metal-Organic Frameworks with Multifunctional Properties for Nitroaromatic Compounds Sensing and Photocatalysis

Fengqin Wang<sup>1\*</sup>, Chengmiao Wang<sup>1</sup>, Zongchao Yu<sup>1</sup>, Qingguo He<sup>2</sup>, Xiuyu Li<sup>1</sup>, Chonglong Shang<sup>1</sup>, Yongnan Zhao<sup>3</sup>

Two luminescent MOFs were employed as multifunctional materials for selectively sensing of nitroaromatic compounds and photodegradation of RhB.

